Article DOI: https://doi.org/10.3201/eid2705.204912

Genetic Evidence and Host Immune Response in Persons Reinfected with SARS-CoV-2, Brazil

Appendix

Detailed Materials and Methods

Measurement of Serum SARS-CoV-2 antibodies

For quantitative analysis of anti-SARS-CoV-2 spike protein IgM, IgA, and IgG antibodies, we performed the S-UFRJ test, as previously described (R.G.F. Alvim et al., unpub. data, https://doi.org/10.1101/2020.07.13.20152884). Briefly, high binding ELISA plates were coated with 50 μL of SARS-CoV-2 spike protein (4 μg/mL in phosphate-buffered saline [PBS]) and incubated overnight. The coating solution was removed, and 100 μL of PBS 1% BSA (blocking solution) was added, and the plate was incubated at room temperature (RT) for 1–2 h. The blocking solution was removed, and 50 μL of diluted 1:40 (PBS 1% BSA) patient serum specimens were added; subsequently, the specimens were serially 3-fold diluted in the plate, which was incubated at RT for 2 h. Then, the plate was washed with 150 μL of PBS (5×) and 50 μL of 1:10,000 goat anti-human IgG, IgA, and IgM (Fc)-horseradish peroxidase antibody (SouthernBiotech, https://www.southernbiotech.com) were added, and the plate was incubated for 1.5 h at RT. The plate was washed again with 150 μL of PBS (5×) and then treated with TMB (3,3‘, 5,5; -tetramethylbenzidine) (Scienco, http://www.scienco.bio.br) until the reaction was stopped with 50 μL of HCl 1N. The optical density (OD) was read at 450 nm with 655 nm background compensation in a microplate reader (Bio-Rad Laboratories, Inc., https://www.bio-rad.com).

Quantification of Plasma Cytokine Levels

Plasma samples from the acute and convalescent phases of the 2 episodes of SARS-CoV-2 infection were collected in EDTA-containing tubes. Tubes were placed on ice and aliquoted. Commercial ELISA kits (R&D Systems, https://www.rndsystems.com) were used to measure interferon (IFN)-α, -β and -γ, interleukin (IL)-6, −8 and −10, tumor necrosis factor α (TNF-α) and

induced protein 10 (IP10)/C-X-C motif chemokine ligand 10 (CXCL-10). This panel of mediators provides evidence for host production of antiviral, pro-inflammatory, and regulatory responses.

Plaque Reduction Neutralization Test (PRNT)

To determine serum titers to block SARS-CoV-2 infection, miniaturized PRNT was performed. In brief, human serum was heat-inactivated (30 min, 56°C) before 2-fold serial dilutions (from 1:4 to 1:2,056). Diluted serum specimens were incubated with 100 PFUs (PFU) of SARS-CoV-2 (GenBank accession no. MT710714) for 1 h at 37°C in 96-well plates. Afterward, mixtures of serum and virus were incubated with Vero E6 cells (2×10^4 cell/well) in 96-well plates for an additional 1 h at 37°C. Next, a fresh semisolid medium containing 2.4% of carboxymethylcellulose (CMC) was added to the wells, and cultures were maintained for 72 h at 37°C. Cells were fixed with 10% formalin for 2 h at room temperature and stained with crystal violet (0.4%). Endpoint dilution inhibiting 90% PFU ($PRNT_{90}$) was scored. As a control, to validate each assay, a back-titration of the mock-treated virus was included. Our quality control accepts the final readout of the virus input to be equivalent to 100 ± 20 PFU. Plaque numbers were scored in ≥ 3 independent experiments with technical replicates by 2 independent blinded readers to determine the $PRNT_{90}$ (Appendix Figure 1).

Molecular Diagnosis

The total viral RNA was extracted using QIAamp Viral RNA (QIAGEN, https://www.qiagen.com), according to the manufacturer's instructions. Quantitative RT-PCR was performed using GoTaq Probe qPCR and RT-qPCR Systems (Promega, https://www.promega.com) in a StepOne Real-Time PCR System (Thermo Fisher Scientific, https://www.thermofisher.com). Amplifications were carried out in 25 µL reaction mixtures containing 2× reaction mix buffer, 50 µM of each primer, 10 µM of the probe, and 5 µL of RNA template. Primers, probes, and cycling conditions used to detect the SARS-CoV-2 RNA were those recommended by the US Centers for Disease Control and Prevention (CDC) (*1*). The standard curve method was employed for virus quantification, using synthetic RNA for gene N (Microbiologics, Minnesota, USA). The C_t values for this target were compared with those obtained with different cell amounts (10^7 to 10^2), for reaction calibration.

Genomic Analysis

Total viral RNA from nasopharyngeal swabs was extracted using QIAamp Viral RNA (QIAGEN), with minor modifications (*2*). In brief, extraction was performed in 2 mL of sample/lysis buffer (1:1) without RNA carrier, and purified RNA was obtained after binding and

elution from a single silica column. For better yields, a 50-µL eluate was repetitively loaded (4×) to the same column. Tests were performed to evaluate if digestion with DNase I and depletion of rRNA enhanced the quantity/quality of SARS-CoV-2-related reads. Samples negative for SARS-CoV-2 and positive for Zika or chikungunya virus were included as controls.

To improve sequencing readout, an amplicon-based enrichment strategy was carried out with the ATOPlex SARS-CoV-2 Full-Length Genome Panel v1.0 (kindly donated by MGI Tech Co., https://en.mgi-tech.com). For library construction, RNA samples were first quantified with the Qubit RNA BR Assay Kit (Thermo Fisher Scientific), according to the manufacturer's instructions. Approximately 5 ng of each sample were then used as inputs to reverse transcription (RT) reactions, followed by two-step multiplex PCR-based genome amplification and dual adaptor indexing (i.e., barcoding) using proprietary primer sets. Products were purified with DNA Clean beads at a 5:6 volume ratio and subsequent washing steps with 80% ethanol. Next, individual libraries were quantified with the Qubit 1X dsDNA HS Assay Kit (Thermo Fisher Scientific) and homogeneously pooled to a total sum of 400 ng, before being submitted to denaturation, circularization, and digestion steps. Finally, single-stranded circular DNA library pools were converted to DNA nanoballs by rolling circle amplification and submitted to pair-end sequencing (100 nt) on the MGISEQ-2000 platform (recently named as DNBSEQ-G400; MGI Tech Co. Ltd).

Genomic sequences were quality-scored, filtered, trimmed, and assembled in contigs through a validated workflow for SARS-CoV-2 (*3*). Genomes were aligned with MAFFT (*4*) or ClustalW (*5*), and phylogenies were constructed with MEGA version 7.0 (*6,7*), using the Jukes-Cantor model for Maximum likelihood estimates, by applying neighbor-join and BioNJ algorithms (*8*). The tree with the highest log-likelihood was used. Alternatively, MrBayes version 3.2.7 (http://nbisweden.github.io/MrBayes) was used for Bayesian inference (*9,10*) with a relaxed clock model with a priori model testing using the gamma rates and invariant sites (G + I) nucleotide substitution model, selected by jModelTest version 1.6 http://darwin.uvigo.es/software/jmodeltest.htm (*11,12*). The tree was visualized and edited with FigTree version 1.4.2 (http://tree.bio.ed.ac.uk). SARS-CoV-2 clades were determined using the Web site https://clades.nextstrain.org. To categorize mutations and polymorphisms, the SARS-CoV-2 reference genome Wuhan-Hu-1 (GISAID EPI ISL no. 402125) was aligned to our sequences. The original sequences used in this work are publicly available on https://www.gisaid.org: GISAID EPI ISL nos. 636737, 636834–636838. The dataset included in the analysis contained representative sequences of the emerging clades associated with our

sequences, 19A and 20B, as well as sequences from the genome 20A as a negative control (Appendix Table 1).

References

1. Centers for Disease Control and Prevention. Research use only 2019-novel coronavirus (2019-nCoV) real-time RT-PCR primers and probes. 2020 [cited 2020 Nov 11]. https://www.cdc.gov/coronavirus/2019-ncov/lab/rt-pcr-panel-primer-probes.html

2. Metsky HC, Matranga CB, Wohl S, Schaffner SF, Freije CA, Winnicki SM, et al. Zika virus evolution and spread in the Americas. Nature. 2017;546:411–5. PubMed https://doi.org/10.1038/nature22402

3. Cleemput S, Dumon W, Fonseca V, Abdool Karim W, Giovanetti M, Alcantara LC, et al. Genome Detective coronavirus typing tool for rapid identification and characterization of novel coronavirus genomes. Bioinformatics. 2020;36:3552–5. PubMed https://doi.org/10.1093/bioinformatics/btaa145

4. Katoh K, Kuma K, Toh H, Miyata T. MAFFT version 5: improvement in accuracy of multiple sequence alignment. Nucleic Acids Res. 2005;33:511–8. PubMed https://doi.org/10.1093/nar/gki198

5. Larkin MA, Blackshields G, Brown NP, Chenna R, McGettigan PA, McWilliam H, et al. Clustal W and Clustal X version 2.0. Bioinformatics. 2007;23:2947–8. PubMed https://doi.org/10.1093/bioinformatics/btm404

6. Kumar S, Stecher G, Li M, Knyaz C, Tamura K. MEGA X: Molecular Evolutionary Genetics Analysis across computing platforms. Mol Biol Evol. 2018;35:1547–9. PubMed https://doi.org/10.1093/molbev/msy096

7. Felsenstein J. Confidence limits on phylogenies: an approach using the bootstrap. Evolution. 1985;39:783–91. PubMed https://doi.org/10.1111/j.1558-5646.1985.tb00420.x

8. Jukes TH, Cantor CR. Evolution of protein molecules. In: Mammalian protein metabolism. Vol. III. H. N. Munro, editor. New York: Academic Press; 1969. p. 21–132.

9. Huelsenbeck, J P, Ronquist F. MRBAYES: Bayesian inference of phylogeny. Bioinformatics. 2001;17:754–755

10. Ronquist, F, Huelsenbeck JP. MRBAYES 3: Bayesian phylogenetic inference under mixed models. Bioinformatics 2003;19:1572–1574.

11. Darriba D, Taboada GL, Doallo R, Posada D. jModelTest 2: more models, new heuristics and parallel computing. Nature Methods. 2012;9:772.

12. Guindon S, Gascuel O. A simple, fast and accurate method to estimate large phylogenies by maximum-likelihood. Systematic Biology. 2003;52:696–704

Appendix Table 1. Access codes for sequences used in tree construction compared with patients' virus sequences in study of patients reinfected with severe acute respiratory coronavirus 2, Brazil, 2020

No.	Name	Accession code
1	hCoV-19/Wuhan/Hu-1/2019	EPI_ISL_402125
2	hCoV-19/Brazil/RJ-UFRJ-9331/2020|EPI_ISL_492036|2020–06–01	EPI_ISL_492036
3	hCoV-19/Brazil/RJ-INCA-C44/2020|EPI_ISL_513551|2020–04–17	EPI_ISL_513551
4	hCoV-19/Brazil/RJ-INCA-C39/2020|EPI_ISL_513547|2020–04–17	EPI_ISL_513547
5	hCoV-19/Brazil/RJ-INCA-C38/2020|EPI_ISL_513546|2020–04–17	EPI_ISL_513546
6	hCoV-19/Brazil/RJ-INCA-C37/2020|EPI_ISL_513545|2020–04–16	EPI_ISL_513545
7	hCoV-19/Brazil/RJ-INCA-C36/2020|EPI_ISL_513544|2020–04–16	EPI_ISL_513544
8	hCoV-19/Brazil/RJ-INCA-C34/2020|EPI_ISL_513542|2020–04–16	EPI_ISL_513542
9	hCoV-19/Brazil/RJ-INCA-C33/2020|EPI_ISL_513541|2020–04–16	EPI_ISL_513541
10	hCoV-19/Brazil/RJ-INCA-C31/2020|EPI_ISL_513539|2020–04–16	EPI_ISL_513539
11	hCoV-19/Brazil/RJ-INCA-C30/2020|EPI_ISL_513538|2020–04–16	EPI_ISL_513538
12	hCoV-19/Brazil/RJ-INCA-C29/2020|EPI_ISL_513537|2020–04–16	EPI_ISL_513537
13	hCoV-19/Brazil/RJ-INCA-C27/2020|EPI_ISL_513535|2020–04–16	EPI_ISL_513535
14	hCoV-19/Brazil/RJ-INCA-C25/2020|EPI_ISL_513533|2020–04–16	EPI_ISL_513533
15	hCoV-19/Brazil/RJ-INCA-C24/2020|EPI_ISL_513532|2020–04–16	EPI_ISL_513532
16	hCoV-19/Brazil/RJ-INCA-C23/2020|EPI_ISL_513531|2020–04–16	EPI_ISL_513531
17	hCoV-19/Brazil/RJ-INCA-C22/2020|EPI_ISL_513530|2020–04–16	EPI_ISL_513530
18	hCoV-19/Brazil/RJ-INCA-C14/2020|EPI_ISL_513517|2020–04–14	EPI_ISL_513517
19	hCoV-19/Brazil/RJ-INCA-C13/2020|EPI_ISL_513516|2020–04–14	EPI_ISL_513516
20	hCoV-19/Brazil/RJ-INCA-C12/2020|EPI_ISL_513515|2020–04–14	EPI_ISL_513515
21	hCoV-19/Brazil/RJ-INCA-C07/2020|EPI_ISL_513514|2020–04–08	EPI_ISL_513514
22	hCoV-19/Brazil/RJ-INCA-C06/2020|EPI_ISL_513513|2020–04–08	EPI_ISL_513513
23	hCoV-19/Brazil/RJ-DCVN1/2020|EPI_ISL_509434|2020–03–23	EPI_ISL_509434
24	hCoV-19/Brazil/RJ-899/2020|EPI_ISL_456071|2020–03–30	EPI_ISL_456071
25	hCoV-19/Brazil/RJ-2072/2020|EPI_ISL_456104|2020–04–16	EPI_ISL_456104
26	hCoV-19/Brazil/RJ-1921/2020|EPI_ISL_456091|2020–04–09	EPI_ISL_456091
27	hCoV-19/Brazil/RJ-1719/2020|EPI_ISL_456088|2020–04–06	EPI_ISL_456088
28	hCoV-19/Brazil/RJ-1702/2020|EPI_ISL_456087|2020–04–08	EPI_ISL_456087
29	hCoV-19/Brazil/RJ-1690/2020|EPI_ISL_456084|2020–04–08	EPI_ISL_456084
30	hCoV-19/Brazil/RJ-1627/2020|EPI_ISL_456083|2020–04–03	EPI_ISL_456083
31	hCoV-19/Brazil/RJ-1595/2020|EPI_ISL_467346|2020–04–02	EPI_ISL_467346
32	hCoV-19/Brazil/RJ-1555/2020|EPI_ISL_467344|2020–04–02	EPI_ISL_467344
33	hCoV-19/Brazil/GO-L19-CD410/2020|EPI_ISL_476333|2020–04–02	EPI_ISL_476333
34	hCoV-19/Brazil/PR-5620/2020|EPI_ISL_541343|2020–03–20	EPI_ISL_541343
35	hCoV-19/Brazil/SP-193/2020|EPI_ISL_523984|2020–04–19	EPI_ISL_523984
36	hCoV-19/Brazil/SP-240/2020|EPI_ISL_524468|2020–05–01	EPI_ISL_524468
37	hCoV-19/Brazil/PE-IAM1126/2020|EPI_ISL_572379|2020–05–07	EPI_ISL_572379
38	hCoV-19/Brazil/SC-L15-CD265/2020|EPI_ISL_476259|2020–03–29	EPI_ISL_476259
39	hCoV-19/Brazil/SP-L14-CD257/2020|EPI_ISL_476253|2020–03–27	EPI_ISL_476253
40	hCoV-19/Brazil/SC-0244/2020|EPI_ISL_470653|2020–03–18	EPI_ISL_470653
41	hCoV-19/Brazil/AL-837/2020|EPI_ISL_427292|2020–03–18	EPI_ISL_427292
42	hCoV-19/Brazil/SP-294/2020|EPI_ISL_527862|2020–03–30	EPI_ISL_527862
43	hCoV-19/Brazil/SP-L5-CAMPI91/2020|EPI_ISL_476419|2020–04–23	EPI_ISL_476419
44	hCoV-19/Brazil/SP-254/2020|EPI_ISL_524469|2020–05–05	EPI_ISL_524469
45	hCoV-19/Brazil/SP-436/2020|EPI_ISL_603033|2020–07–13	EPI_ISL_603033
46	hCoV-19/Brazil/SP-441/2020|EPI_ISL_603038|2020–07–20	EPI_ISL_603038
47	hCoV-19/Brazil/RS-0242/2020|EPI_ISL_470651|2020–03–20	EPI_ISL_470651
48	hCoV-19/Brazil/SP-356/2020|EPI_ISL_547575|2020–06–16	EPI_ISL_547575
49	hCoV-19/Brazil/SP-321/2020|EPI_ISL_534316|2020–05–02	EPI_ISL_534316
50	hCoV-19/South_Korea/KCDC2712/2020|EPI_ISL_522491|2020–07–11	EPI_ISL_522491
51	hCoV-19/Brazil/PR-5621/2020|EPI_ISL_541344|2020–03–19	EPI_ISL_541344
52	hCoV-19/Brazil/SP-437/2020|EPI_ISL_603034|2020–07–11	EPI_ISL_603034
53	hCoV-19/Brazil/SP-433/2020|EPI_ISL_603030|2020–07–11	EPI_ISL_603030
54	hCoV-19/Brazil/UN-HIAE-SP04/2020|EPI_ISL_486429|2020–03–20	EPI_ISL_486429
55	hCoV-19/Norway/3069/2020|EPI_ISL_549084|2020–08–10	EPI_ISL_549084
56	hCoV-19/Brazil/SP-370/2020|EPI_ISL_583500|2020–06–29	EPI_ISL_583500
57	hCoV-19/Brazil/RJ-UFRJ-9331/2020|EPI_ISL_492036|2020–06–01	EPI_ISL_492036
58	hCoV-19/Thailand/Bangkok-0071/2020|EPI_ISL_445380|2020–03–30	EPI_ISL_445380
59	hCoV-19/Brazil/SP-439/2020|EPI_ISL_603036|2020–07–10	EPI_ISL_603036
60	hCoV-19/Brazil/SP-440/2020|EPI_ISL_603037|2020–07–20	EPI_ISL_603037
61	hCoV-19/Brazil/SP-394/2020|EPI_ISL_583503|2020–06–22	EPI_ISL_583503
62	hCoV-19/Brazil/SP-398/2020|EPI_ISL_603028|2020–06–30	EPI_ISL_603028
63	hCoV-19/Brazil/SP-L5-CAMPI77/2020|EPI_ISL_476416|2020–04–23	EPI_ISL_476416

No.	Name	Accession code
64	hCoV-19/Brazil/SP-283/2020|EPI_ISL_527860|2020–04–17	EPI_ISL_527860
65	hCoV-19/Ecuador/USFQ-004/2020|EPI_ISL_477014|2020–03–30	EPI_ISL_477014
66	hCoV-19/Ecuador/USFQ-020/2020|EPI_ISL_471267|2020–04–17	EPI_ISL_471267
67	hCoV-19/Ecuador/USFQ-039/2020|EPI_ISL_481245|2020–04–17	EPI_ISL_481245
68	hCoV-19/Ecuador/USFQ-1112/2020|EPI_ISL_486847|2020–06–30	EPI_ISL_486847
69	hCoV-19/Ecuador/USFQ-110/2020|EPI_ISL_486845|2020–06–30	EPI_ISL_486845
70	hCoV-19/Italy/APU-UniMI-123PT/2020|EPI_ISL_525554|2020–07–20	EPI_ISL_525554
71	hCoV-19/Brazil/GO-L19-CD413/2020|EPI_ISL_476336|2020–04–02	EPI_ISL_476336
72	hCoV-19/Brazil/MG-0288/2020|EPI_ISL_470593|2020–04–09	EPI_ISL_470593
73	hCoV-19/Brazil/RJ-0251/2020|EPI_ISL_470619|2020–03–27	EPI_ISL_470619
74	hCoV-19/Brazil/GO-0209/2020|EPI_ISL_470576|2020–04–03	EPI_ISL_470576
75	hCoV-19/Argentina/PAIS-A0023/2020|EPI_ISL_430814|2020–04–17	EPI_ISL_430814
76	hCoV-19/Luxembourg/LNS9470500/2020|EPI_ISL_434505|2020–04–08	EPI_ISL_434505
77	hCoV-19/Mexico/HID-InDRE-54/2020|EPI_ISL_576257|2020–07–22	EPI_ISL_576257
78	hCoV-19/Mexico/CMX-INMEGEN-02/2020|EPI_ISL_522873|2020–07–31	EPI_ISL_522873
79	hCoV-19/Peru/LIM-UPCH-0146/2020|EPI_ISL_568540|2020–08–28	EPI_ISL_568540
80	hCoV-19/Peru/LIM-INS-138/2020|EPI_ISL_536533|2020–03–17	EPI_ISL_536533
81	hCoV-19/Peru/LIM-INS-078/2020|EPI_ISL_536478|2020–07–02	EPI_ISL_536478
82	hCoV-19/Peru/LIM-UPCH-0160/2020|EPI_ISL_568553|2020–08–28	EPI_ISL_568553
83	hCoV-19/CotedIvoire/BKE0891/2020|EPI_ISL_614389|2020–08–18	EPI_ISL_614389
84	hCoV-19/Peru/LIM-INS-120/2020|EPI_ISL_536518|2020–05–05	EPI_ISL_536518
85	hCoV-19/Peru/LIM-UPCH-0138/2020|EPI_ISL_568534|2020–08–27	EPI_ISL_568534
86	hCoV-19/Turkey/KOC-IST-OD5/2020|EPI_ISL_613460|2020–06–21	EPI_ISL_613460
87	hCoV-19/USA/WI-UW-1054/2020|EPI_ISL_516480|2020–07–30	EPI_ISL_516480
88	hCoV-19/USA/WI-UW-759/2020|EPI_ISL_495464|2020–07–06	EPI_ISL_495464
89	hCoV-19/Peru/LIM-UPCH-0147/2020|EPI_ISL_568541|2020–08–28	EPI_ISL_568541
90	hCoV-19/USA/MI-MDHHS-SC22181/2020|EPI_ISL_614232|2020–10–12	EPI_ISL_614232
91	hCoV-19/USA/VA-DCLS-1506/2020|EPI_ISL_581508|2020–07–28	EPI_ISL_581508
92	hCoV-19/Peru/LIM-INS-100/2020|EPI_ISL_536499|2020–07–04	EPI_ISL_536499
93	hCoV-19/Mexico/CMX-INMEGEN-03/2020|EPI_ISL_522874|2020–07–31	EPI_ISL_522874
94	hCoV-19/Peru/LIM-UPCH-0127/2020|EPI_ISL_568523|2020–08–28	EPI_ISL_568523
95	hCoV-19/Peru/LIM-UPCH-0129/2020|EPI_ISL_568525|2020–08–28	EPI_ISL_568525
96	hCoV-19/Peru/LIM-UPCH-0128/2020|EPI_ISL_568524|2020–08–28	EPI_ISL_568524
97	hCoV-19/Romania/Mioveni-24095/2020|EPI_ISL_468156|2020–05–08	EPI_ISL_468156
98	hCoV-19/Mexico/TLA-InDRE-57/2020|EPI_ISL_576260|2020–08–13	EPI_ISL_576260
99	hCoV-19/Mexico/ZAC-InDRE-72/2020|EPI_ISL_576275|2020–08–14	EPI_ISL_576275
100	hCoV-19/France/BRE-BR9068/2020|EPI_ISL_613557|2020–09–06	EPI_ISL_613557
101	hCoV-19/Singapore/1110/2020|EPI_ISL_605819|2020–10–25	EPI_ISL_605819
102	hCoV-19/Netherlands/ZH-EMC-552/2020|EPI_ISL_577980|2020–09–08	EPI_ISL_577980
103	hCoV-19/Netherlands/ZH-EMC-607/2020|EPI_ISL_578035|2020–09–17	EPI_ISL_578035
104	hCoV-19/Brazil/SP-405/2020|EPI_ISL_547577|2020–07–06	EPI_ISL_547577
105	hCoV-19/Brazil/DF-0001/2020|EPI_ISL_426580|2020–03–13	EPI_ISL_426580
106	hCoV-19/Brazil/SP-345/2020|EPI_ISL_583495|2020–06–13	EPI_ISL_583495
107	hCoV-19/Brazil/PI-0239/2020|EPI_ISL_470613|2020–03–19	EPI_ISL_470613
108	hCoV-19/Brazil/RN-IEC-162277/2020|EPI_ISL_524798|2020–03–14	EPI_ISL_524798
109	hCoV-19/Brazil/RJ-INCA-C34/2020|EPI_ISL_513542|2020–04–16	EPI_ISL_513542
110	hCoV-19/Brazil/DF-891/2020|EPI_ISL_427298|2020–03–22	EPI_ISL_427298
111	hCoV-19/Brazil/DF-862/2020|EPI_ISL_427297|2020–03–23	EPI_ISL_427297
112	hCoV-19/Brazil/SP-399/2020|EPI_ISL_603029|2020–06–22	EPI_ISL_603029
113	hCoV-19/Ireland/D-NVRL-72IRL12139/2020|EPI_ISL_528465|2020–08–12	EPI_ISL_528465
114	hCoV-19/Brazil/MG-0291/2020|EPI_ISL_470596|2020–04–16	EPI_ISL_470596
115	hCoV-19/Brazil/RJ-00318/2020|EPI_ISL_623121|2020–05–12	EPI_ISL_623121
116	hCoV-19/Brazil/BA-L17-CD359/2020|EPI_ISL_476305|2020–03–31	EPI_ISL_476305
117	hCoV-19/Brazil/RJ-INCA-C181/2020|EPI_ISL_513519|2020–04–30	EPI_ISL_513519
118	hCoV-19/Brazil/AP-IEC-165669/2020|EPI_ISL_524793|2020–04–29	EPI_ISL_524793
119	hCoV-19/Brazil/RJ-0263/2020|EPI_ISL_470630|2020–04–13	EPI_ISL_470630
120	hCoV-19/Brazil/RJ-00364/2020|EPI_ISL_623167|2020–05–04	EPI_ISL_623167
121	hCoV-19/Brazil/RJ-UFRJ-58271/2020|EPI_ISL_492048|2020–06–01	EPI_ISL_492048
122	hCoV-19/Brazil/DF-615i/2020|EPI_ISL_427294|2020–03–13	EPI_ISL_427294
123	hCoV-19/Spain/GA-IBV-98006079/2020|EPI_ISL_541066|2020–07–03	EPI_ISL_541066
124	hCoV-19/Brazil/RJ-00316/2020|EPI_ISL_623119|2020–05–04	EPI_ISL_623119
125	hCoV-19/Argentina/PAIS-A0024/2020|EPI_ISL_430815|2020–04–18	EPI_ISL_430815
126	hCoV-19/Argentina/Heritas_HG001/2020|EPI_ISL_476496|2020–04–22	EPI_ISL_476496
127	hCoV-19/Argentina/Heritas_HG006/2020|EPI_ISL_476561|2020–05–07	EPI_ISL_476561
128	hCoV-19/Argentina/Heritas_HG007/2020|EPI_ISL_476565|2020–05–09	EPI_ISL_476565
129	hCoV-19/Argentina/Heritas-HG023/2020|EPI_ISL_615121|2020–05–26	EPI_ISL_615121
130	hCoV-19/Brazil/RJ-1466/2020|EPI_ISL_456081|2020–04–06	EPI_ISL_456081
131	hCoV-19/Brazil/RJ0272/2020|EPI_ISL_470638|2020–04–17	EPI_ISL_470638

No.	Name	Accession code
132	hCoV-19/Brazil/RJ0256/2020|EPI_ISL_470624|2020–04–03	EPI_ISL_470624
133	hCoV-19/Brazil/RJ0254/2020|EPI_ISL_470622|2020–04–01	EPI_ISL_470622
134	hCoV-19/Brazil/RJ0251/2020|EPI_ISL_470619|2020–03–27	EPI_ISL_470619
135	hCoV-19/Brazil/RJ0248/2020|EPI_ISL_470616|2020–03–24	EPI_ISL_470616
136	hCoV-19/Brazil/RJ-0720/2020	EPI_ISL_636836
137	hCoV-19/Brazil/RJ-01020/2020	EPI_ISL_636834
138	hCoV-19/Brazil/RJ-06020/2020	EPI_ISL_636737
139	hCoV-19/Brazil/RJ-01020–2/2020	EPI_ISL_636835
140	hCoV-19/Brazil/RJ-0720.2/2020	EPI_ISL_63683
141	hCoV-19/Brazil/RJ-0920/2020	EPI_ISL_63683

Appendix Table 2. Genetic characteristics of the SARS-CoV-2 sequences detected in patients who were infected twice, Brazil, 2020

	First episode of infection		Second episode of infection			
Characteristics of SARS-CoV-2 sequences	Patient B (% quasispecies)	Patient C (% quasispecies)	Patient A (% quasispecies)	Patient B (% quasispecies)	Patient C (% quasispecies)	Patient D (% quasispecies)
No. reads	>140K	>2.600K	>472K	>24.400K	>15.600K	>20.000K
Phred quality score	-Q35	-Q36	-Q33	-Q36	-Q36	-Q36
Depth of coverage, average ± SD	103.5 ± 1.24	2018.85 ± 31.53	350.85 ± 4.04	18426.125 ± 279.91	11753.53 ± 257.32	10061.58 ± 3701.20
Mutations						
NSP2 (AA)						
G1522A (none)	X					
NSP3 (AA)						
A6866G (N1383D)	X					
C3037T (none)	X	X (24.7)	X	X	X	X
C6021T (P1101L)	X (25.44)					
4151_4152delTT (L478X)		X				
C7164T (T1482I)		X (25.1)				
T7082A (S1455T)			X (25.3)			
A7384T (Q1555H)			X (25.3)			
NSP4 (AA)						
C9569T (P339S)			X (25.3)			
3C-like proteinase (AA)						
A10904G (S284G)		X (25.1)				
NSP6 (AA)						
C11514T (T181I)			X	X	X	X
RNA-dependent RNA polymerase (AA)						
G15406T (A656S)	X					
C14408T (P323L)	X (74.6)	X	X	X	X	X
A14836G (I466V)	X (24.77)					
Helicase (AA)						
A17105G (H290R)			X (25.3)			
3′-5′-Exonuclease						
G18412T (V125F)			X	X	X	X
G18180T (K47N)						X
18180_18181insTG (K47_D48insX)						X
EndoRNase						
A20265G (none)	X (25.44)					
2'-O-Ribose methyltransferase						
A21415T (K53*)	X (24.76)					
Surface glycoprotein						
A23403G (D614G)	X	X	X	X	X	X
T22619G (W353G)			X (25.3)			
Membrane glycoprotein						
G26795T (M91I)	X					
G27112A (S197N)	X (25.01)					
A26555N (E11X)	X (25.44)					
G26556N /A26557N/ G26558N (E12X)	X (25.44)					
C26559N (L13X)	X (25.44)					
27184_27228del TACAGTAAGTGACAA CAGATGTTTCATCTCGTTGACTTTCAGGTT (V221X)				X (24.7)		

	First episode of infection		Second episode of infection			
Characteristics of SARS-CoV-2 sequences	Patient B (% quasispecies)	Patient C (% quasispecies)	Patient A (% quasispecies)	Patient B (% quasispecies)	Patient C (% quasispecies)	Patient D (% quasispecies)
ORF6						
T27299C (133T)		X	X	X (75.3)	X	X
27184_27228delTACAGTAAGTGACAACAGATGTTTCATCTCGTTGACTTTCAGGTT (M1_V9del)				X (24.7)		
27196_27228delCAACAGATGTTTCATCTCGTTGACTTTCAGGTT (M1_V9del)					X (24.54)	
27197_27226delAACAGATGTTTCATCTCGTTGACTTTCAGG (M1_Q8del)					X (25.56)	
27197_27226delAACAGATGTTTCATCTCGTTGACTTTCAGG (V9X)					X (25.56)	
A27313G (K38E)						X
Nucleocapsid						
G28881A/G28882G (R203K)		X	X	X	X	X
G28883C (G204R)		X	X	X	X	X
T29148C (I292T)		X	X	X	X	X

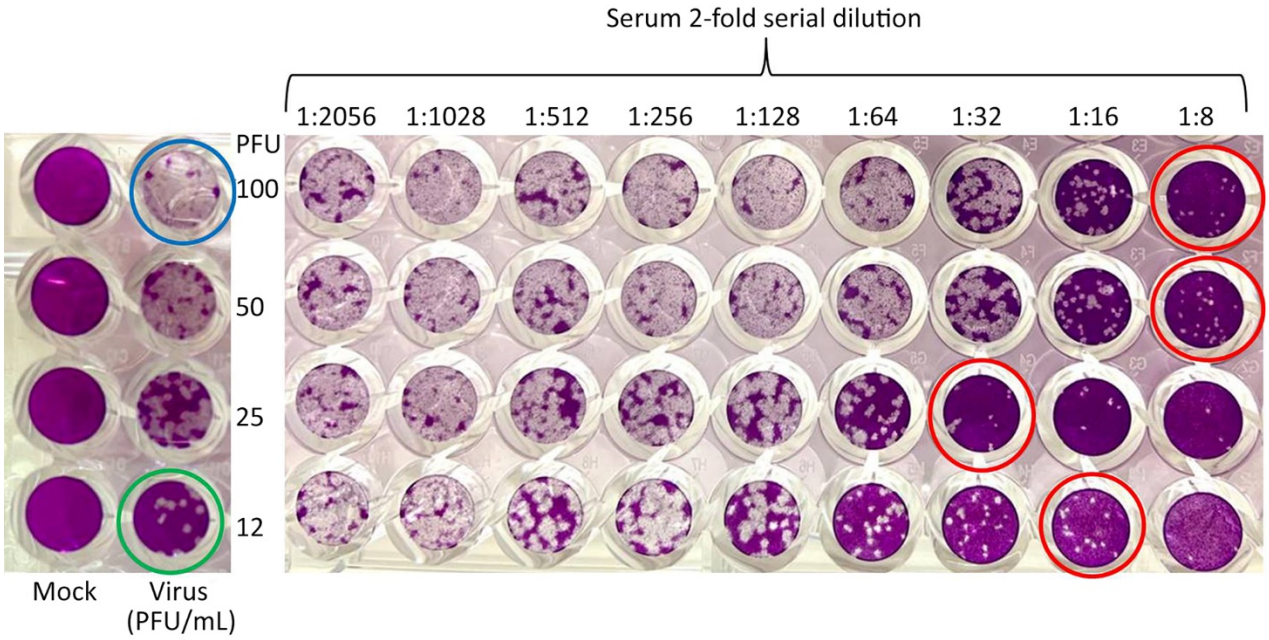

Appendix Figure 1. Representative readout of PRNT. 2-fold serial dilutions (from 1:4 to 1:2056) of human serum specimens were incubated in duplicates with ≈100 PFUs (PFU) of SARS-CoV-2. The serum–virus mixture was incubated for 1 h at 37°C and then added to Vero E6 cells (2×10^4 cell/well) in 96-well plates and incubated for an additional 1 h at 37°C. Next, a medium with 2.4% CMC was added. After 72 h at 37°C, cells are fixed with 10% formalin and stained with crystal violet (0.4%). Mock = uninfected control. To calculate virus PFU/mL, a back-titration of the mock-treated virus was included in each experiment, the undiluted virus input incubated with the serum is highlighted by the blue circle, a 2-fold serial dilution of the virus is shown, the last dilution of the virus input (1:8) produced 12/13 PFU (green circle), validating the assay. The endpoint dilution of the serum capable of neutralizing the virus input (blue circle) by 90% was expected to produce ≈10 PFU; these dilutions are shown by the red circles.

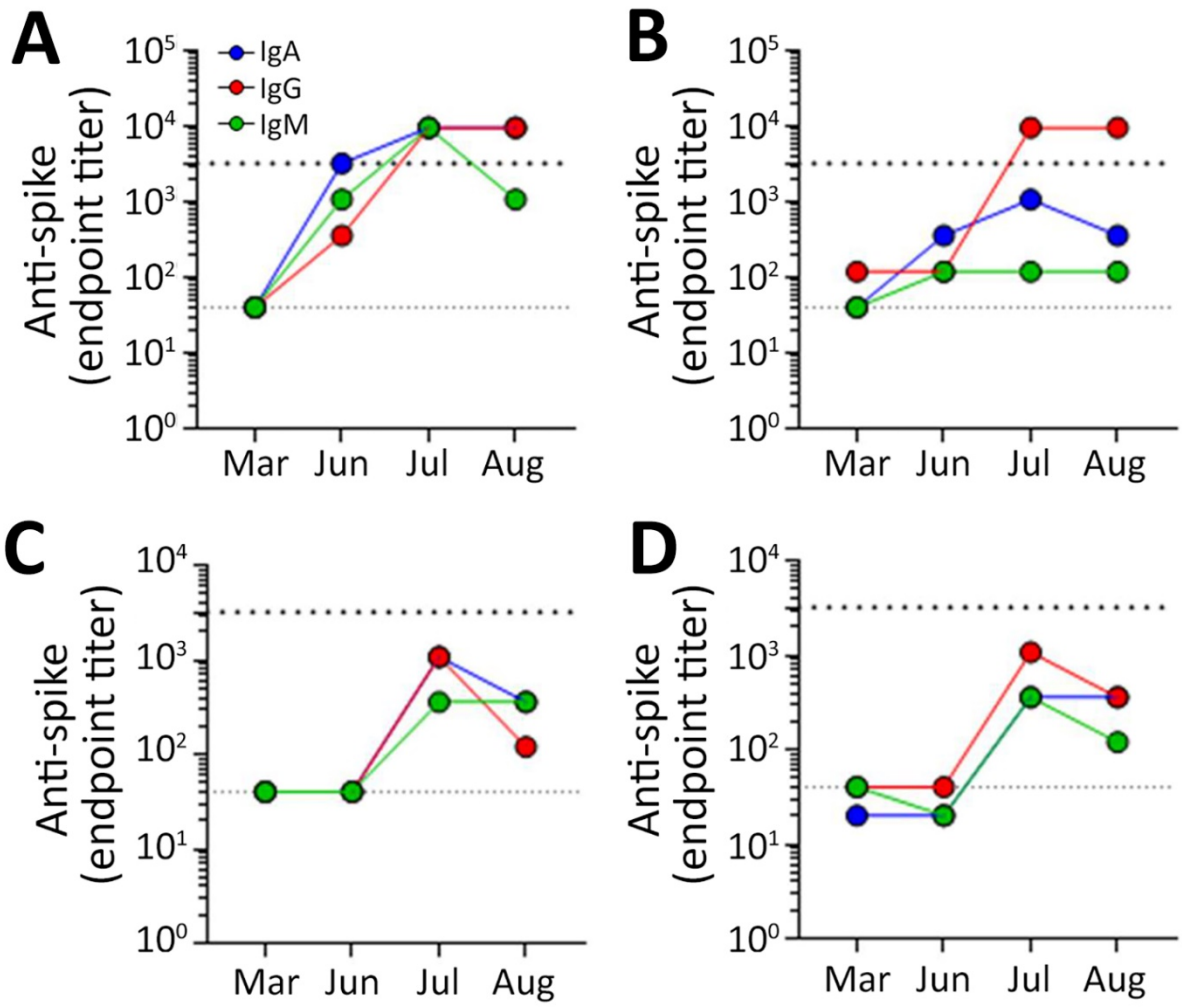

Appendix Figure 2. Quantitative analysis of IgA, IgM, and IgG from patients during the primary, second infections, and 2 months after the second infection. Plasma samples from patients were collected in March, June, July, and August for longitudinal detection of anti-Spike IgM (green), IgA (blue), and IgG (red) antibodies (A–D). The relative levels of antibodies were shown as endpoint titers of patient sample values for optical density [mean + 3 standard deviation (X + 3SD)] negative controls on the same ELISA plate. The dashed horizontal line represents the endpoint titer value between 10,000–30,000. The samples below the dotted line are considered negative.

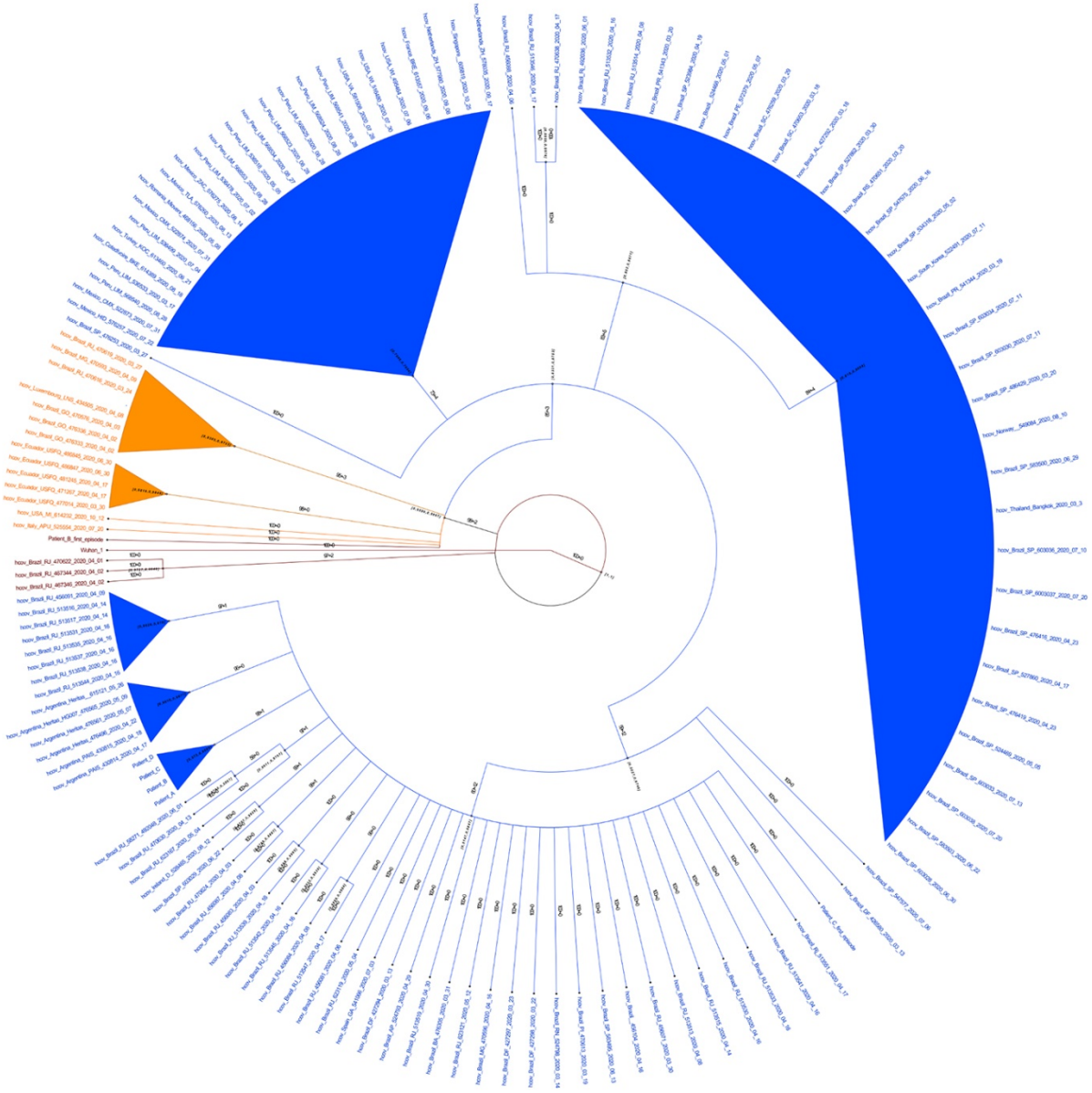

Appendix Figure 3. Phylogeny constructed by Bayesian inference using MrBayes version 3.2.7 (http://nbisweden.github.io/MrBayes), assuming a relaxed clock model with a priori model testing using the gamma rates and invariant sites nucleotide substitution model, selected by jModelTest version 1.6 (https://github.com/ddarriba/jmodeltest2). Emerging clade 19A is brown, clade 20A is orange, and clade 20B is blue. Posterior and anterior probabilities are presented for each branch.